Research on UPQC Harmonic Control Strategy Based on Optimized QPIR Controller of Beetle Antennae Search Algorithm in Microgrid

Hu Jian
NI Fuyin (7896276@qq.com)

Research Article

Keywords: Microgrid, Unified power quality conditioner, Harmonic control, Quasi-PIR control

Posted Date: May 16th, 2023

DOI: https://doi.org/10.21203/rs.3.rs-2915365/v1

Additional Declarations: No competing interests reported.

Version of Record: A version of this preprint was published at Electrical Engineering on October 27th, 2023. See the published version at https://doi.org/10.1007/s00202-023-02066-0.

Abstract

It is difficult to achieve low-order harmonic tracking control without static difference when PI control is used in unified p-ower quality conditioner (UPQC). What's more, the traditional PI parameter trial method has the problems such as low accuracy and anti-interference to meet the needs of real time control. Aiming at this issue, this paper proposes a UPQC harmonic control method based on the beetle antennae search (BAS) algorithm to optimize the parameters of quasi-proportional integral resonance (QPIR) controller. The harmonic current is detected by the i_p-i_q method based on the instantaneous power theory, and the detected signal is input to the QPIR controller. The controller parameters are optimized by the BAS algorithm to improve the dynamic response performance and control accuracy of the UPQC. Then use the MATLAB/Simulink software platform to build UPQC simulation models for PV and wind microgrids. Finally, the simulation comparison is verified between the optimized QPIR controller strategy based on by BAS method and PI control strategy based on neural network algorithm (NNA)respectively. The results show that use QPIR controller optimized through the beetle antennae search (BAS) method is more accurate and resistant to interference. So, the proposed UPQC control strategy has innovation and feasibility, and it can be applied in the practical engineering.

Introduction

A microgrid power generation system comprising of distributed power sources, loads, and energy storage systems has garnered attention worldwide due to the increasing energy crisis and environmental degradation[1]. Microgrid utilizes various types of distributed energy sources such as wind, light, and natural gas to complement each other and has a higher ratio of new energy access. Although microgrid has advantages over traditional large grids, it still has some disadvantage[2]. For instance, loads mostly use various types of converters due to the rapid development of power electronics, and these nonlinear loads not only absorb a large amount of reactive power but also act as harmonic sources, increasing the harmonic content in the grid current[3]. Hence, harmonic management in microgrid, particularly at the Public of Common Coupling (PCC) of microgrid and large grid, has become a hot topic of research[4]. The Unified Power Quality Conditioner (UPQC) is an integrated power quality management device that can suppress voltage dips, unbalance and harmonics, and compensate current harmonics. Therefore, UPQC is widely used for harmonic management in microgrid[5][6].

To address the problem of harmonic suppression in microgrids, various control strategies have been proposed in literature. One approach is to use the comprehensive control strategy of harmonic governance of energy storage systems[7][10]. However, the literature[8] lacks consideration for the capacity limitation of the energy storage system and selective compensation for specific subharmonics, resulting in poor harmonic governance.

Another approach is to use control algorithms to suppress harmonics of the power grid[11][14]. For instance, literature[12] proposes a resonance control based on PID, but fails to consider tuning design of resonant controller parameters. A UPQC that combines PI and PR control algorithms has also been used

to suppress harmonic problems in microgrids [15][20]. Although literature[16] proposes a method based on UPQC and Static Var Compensator (SVC) operation to improve power quality, its control accuracy and response speed are not high.

A method for compensating harmonics in microgrids based on multi-inverter distributed power supply coordination has been proposed, which can output fundamental power while compensating harmonics and improving power quality[21][23]. Although this method is effective in addressing the internal harmonic problem of microgrids, it has a complex structure and is difficult to control.

To tackle the aforementioned issues, this study proposes a UPQC harmonic control method based on the Beetle Antennae Search (BAS) algorithm [24]to optimize the quasi-proportional integral resonance (QPIR) controller parameters. Compared to the traditional PI control method, QPIR control exhibits higher dynamic response performance and control accuracy, which can enhance system stability, reduce sensitivity, and suppress harmonics in the AC current. The BAS algorithm is used for QPIR controller parameter adjustment, and the algorithm's computational results are stable, preventing the problem of premature convergence while significantly reducing the number of operations. In addition, the proposed method employs a current harmonic detection technique as the detection method of UPQC, which addresses the low accuracy and deviation from the actual value issues associated with traditional p-q harmonic detection methods. These improvements enhance the dynamic response performance and control accuracy of UPQC. A MATLAB/Simulink software platform is used to build a UPQC simulation model to verify the proposed control strategy's correctness and feasibility under various microgrid test environments.

1 UPQC parallel unit mathematical model

In this paper, QPIR control method based on the Beetle Antennae Search algorithm is used for harmonic current compensation on the shunt side of the UPQC. The UPQC shunt compensation unit is a back-to-back voltage converter, and the topology circuit diagram of the shunt unit connected to the grid and the load is shown in Fig. 1 .

In the Fig. 1, u_{2K} and i_{sK} are the three-phase AC load voltage and current, respectively, i_{CK2} is the three-phase current on the AC side of the converter, and R and L2 are the series compensation inductor and resistance, where k = a, b, c. Define the binary logic switching function of the shunt unit converter, where k = a, b, c correspond to the A2, B2, C2 three-phase bridge arms of the series converter, respectively.

As shown in Fig. 1, assuming that the voltage U_{dc}on the DC side is a constant value, the relationship between the voltage on the AC side of the parallel unit with respect to the reference point N on the DC side and U_{dc} can be obtained according to the VSC2 inverter circuit.

The three-phase circuit equations described by the switching function are established for the compensation inductor and filter capacitor respectively, and the mathematical model of the UPQC parallel.

2 UPQC current harmonic detection

The accuracy and real time of voltage and current compensation detection of the UPQC is an important part of its integrated compensation. This paper use the i_p- i_q harmonic detection method based on instantaneous power theory, which can accurately detect harmonics and reactive currents in the case of asymmetric and distorted grid voltages, realizing the accuracy and real time of voltage and current distortion detection process of UPOC, and the principle diagram of harmonic current detection and compensation is shown in Fig. 2.

i_L means the three-phase load current, i_h means the three-phase compensation current, and the current i_h^* is generated through QPIR control, and the voltage u_k is output by space vector pulse width modulation(SVPWM)and the compensation current i_m is output by parallel active power filter(PAPF)power driver module for harmonic compensation.

When using the i_p- $i_q$detection method for compensation amount detection, the phase of the A-phase voltage needs to be extracted first, and then the sine cosine signal is obtained through the sine cosine signal generation circuit. In the actual detection process, the phase of the A-phase grid voltage $u_a$can be obtained through the phase-locked loop, and then the sine cosine signal of the same phase of the A-phase grid voltage is obtained through the sine cosine signal generation circuit. The instantaneous value of active current component $i_p$and instantaneous value of reactive component $i_q$can be obtained by multiplying the current components on the $\alpha - \beta$axis with the transformation matrix C. The detection principle is shown in Fig. 3.

The sine signal sin(t) and the corresponding cosine signal -cos(t) of the same frequency and phase as the voltage of phase on the network side are obtained through the phase-locked loop, and then the sampled values of the load currentsi_a i_b i_c are matrix transformed to obtain the corresponding three-phase instantaneous active currents and reactive currents .

3 UPQC harmonic control strategy of quasi-PIR controller based on Beetle Antennae Search algorithm

(1)Harmonic control strategy of UPQC based on quasi-PIR controller

To achieve PI control in current with harmonics, static difference tracking is not possible. Instead, PR controller can suppress low harmonics effectively. However, when applied to actual systems, PR controller faces two problems. Firstly, analog components have relatively low accuracy compared to digital systems. Secondly, PR controller has very small gain in non-basic frequency, leading to poor grid harmonic suppression when grid frequency shifts. To address these issues, an easy to implement QPR controller is proposed based on PR controller. The QPR controller considers static-free tracking of *d* and q-axis dc active components and effectively suppresses lower harmonic currents. The UPQC system is designed to provide the highest filtering compensation for the harmonic. Therefore, multiple QPIR

controllers are required to take compensation control for specific harmonics, and the block diagram of the QPIR control is shown in Fig. 4 .

Therefore, the transfer function of the quasi-PIR controller is shown in Eq. (1).

$$G_{QPIR}(s) = k_p + \frac{k_i}{s} + \sum_{n=6,12,18} \frac{2k_r\omega_c s}{s^2 + 2\omega_c s + (n\omega)^2}$$

1

In the above equation, k_p k_i and k_r are the proportional, integral, and resonant

coefficients, respectively; $\omega_c$and $\omega_0$are the cutoff and resonant frequencies. The resonant frequency is set to the resonant frequency to be eliminated by taking advantage of the infinite gain at the resonant frequency ω_0, so that the current deviation value can be amplified and the input signal can be tracked without static difference and filtered for a specific frequency harmonic.

The closed-loop transfer function of the d-axis current loop can be obtained from the figure as shown in Eq. (2).

$$G_I(s) = \frac{G_{QPIR}(s)K_{PWM}(s)}{L_2 s + R_2 + G_{PIR}(s)K_{PWM}(s)}$$

2

In the above Eq. (2). Substituted into the equation, and let $s = j\omega_0$, then the closed-loop transfer function expression can be derived as shown in Eq. (3).

$$G_I(s) = \frac{K_{PWM}(j\omega_0)}{\frac{Lj\omega_0 + R}{k_p + \frac{k_i}{j\omega_0} + \frac{2k_r j\omega_0}{-{\omega_0}^2 + {\omega_0}^2}} + K_{PWM}(j\omega_0)} \approx 1$$

3

The amplitude of the transfer function is shown in Eq. (4).

$$A(j\omega_0) = \left| k_p + \frac{k_i}{j\omega_0} + \frac{2k_r j\omega_0}{-{\omega_0}^2 + {\omega_0}^2} \right| \approx \infty$$

4

The d-axis current is used for analysis, and a simplified control block diagram of the d-axis current loop is designed as shown in Fig. 5.

Since the amplitude of the QPIR controller is infinite at frequencyω_0, $\omega_0$is set to the frequency of the number of harmonics to be eliminated, when there is a corresponding low harmonic frequency in the feedback current, the QPIR controller can infinitely expand the difference between the detected harmonic current and the feedback current, the QPIR control in the closed loop by the role of negative feedback can eliminate the error, as shown by the equation can be closed loop transfer function is approximately 1, making the output current accurately track the control harmonics.

(2)Quasi-PIR controller parameter selection

The parameters of the quasi-PIR controller are k_p k_i k_r ω_c ω_0, where the

cutoff frequency ω_c determines the range of resonant frequency, the larger the ω_c, the greater the frequency range of the resonant region, take the value of 5 to 15 rad/s, this design is selected 5 rad/s, resonant frequency ω_0 determines the frequency of the resonant point, and the number of harmonics to be eliminated, in this elimination of the 4th harmonic, so ω_0 take the value of 1256.637 rad/s.

The three parameter variations k_p k_i and k_r have an impact on the stability of the controller and the system. The selection of parameter thresholds also needs to be derived from the analysis of more parameter values. In the case of k_i $k_r$unchanged, changek_p, with the increase of k_p, the resonant frequency range will be reduced, which will lead to the controller is more sensitive to the fluctuations of the grid and load, if k_p is too small, the phase lag is serious, so k_p should be controlled in the range of 1 to 10.

As k_i increases, the low frequency gain increases, but k_i is too large will also make the phase lag, so the value of k_i taking into account the low frequency gain should be 10 to 100. k_r changes when the gain of the resonant point will change, with k_r increases, the gain of the resonant point increases, the resonant frequency range also increased, but k_r will be too large to make the phase overrun, k_r is too small and will reduce the gain of the resonant point and reduce the resonant range, so the value of k_r should be 10∼100.

(3)Parameter optimization of quasi-PIR controller based on BAS search

A block diagram of the parameter optimization of the quasi-PIR controller based on BAS search is shown in Fig. 6.

The UPQC QPIR controller design scheme involves determining the range of each parameter, rectifying the parameters, and analyzing them using the BAS algorithm. This helps to narrow the range of parameter values and ultimately determine the parameters.

To make the PIR performance parameter index (i.e., the degree of adaptation) optimal, the adaptation function *J* is chosen as shown in Eq. (5).

$$J = \int_0^{+\infty} (\delta_1 |e(t)| + \delta_2 u^2(t) + \delta_3 |e(t)|)dt + \delta_4 t_u$$

5

$e(t) = r(t) - y(t)$ represents the control deviation, where $r(t)$ and $u(t)$ are the input and output control signals of the PIR controller in UPQC. $\delta_1 \sim \delta_4$are the first to fourth weighting coefficients, respectively, taken as δ_1= 1, δ_2=0.002, δ_3 =120, δ_4= 1.5, and t_u is the rise time.

The parameter adjustment process is as follows.

Step 1: Description of the location of the randomly generated aspen and the orientation of the aspen whiskers, normalized as shown in Eq. (6).

$$\overrightarrow{b} = \frac{rands(d,1)}{||rands(d,1)||}$$

6

where the random function is set to $rands(d,1)$,and d denotes the spatial dimension.

Step 2: Establish the expressions of the left and right whiskers of the aspen and the center of mass by the perception of the as-pen tentacles, perform leftward and right-ward searches, calculate the initial J value, and determine whether the value of the adaptation function proceeds in the direction of decreasing *J*. The expressions of the left and right whiskers of the aspen and the center of mass are shown in Eq. (7).

$$\begin{cases} x_{li} = x^t + d_o^t \times \overrightarrow{b}/2 \\ x_{ri} = x^t + d_o^t \times \overrightarrow{b}/2 \end{cases}$$

7

x_{ri} is the position of the right whisker of the aspen at the tth iteration, x_{li} is the position of the right whisker of the aspen at the tth iteration, x^t is the position of the left whisker of the aspen at the tth iteration, and d_o^t is the distance between the two whiskers of the aspen at the tth iteration.

Step 3: Establish the position update iterative model and determine the initial optimal parameters; its position iterative update formula is shown in Eq. (8).

$$\begin{cases} x^{t+1} = x^t - eta^t \times \overrightarrow{b} \times sign(f(x_{ri}) - f(x_{li})) \\ d_o^t = 0.95 d^{t-1} + 0.01 \\ eta^t = 0.95 \times eta^{t-1} \end{cases}$$

8

In the above equation, eta is the step factor of the search, $f(x)$ is the x position, $sign(.)$ is the sign function, and the position and velocity updates of the aspen are calculated using Eq. (9).

$$\begin{cases} X_i^{t+1} = X_i^t - e(t)at \times sign(J(x_{in}) - J(x_{li})) \\ v_i^{t+1} = v_i^t + (x_i^t - x^*) \times (f_{\min} + (f_{\max} - f_{\min}) \times rand(1,d)) \\ y_i^{t+1} = x_i^t + v_i^{t+1} + x_i^{t+1} \end{cases}$$

9

where X_i^t denotes the current iteration position and v_i^t denotes the current iteration speed value.

Step 4: To correct the optimal position of the aspen, compare the calculated adaptation value with the set threshold value. This completes the correction of the global optimal position, and allows for determining if the optimal position has been reached. If not satisfied, return to step 3 to recalculate the objective function value *J*. The flow chart of the algorithm rectification is shown in Fig. 7 .

Use BAS to find the optimal and rectify the 3 parameters of the QPIR controller, the algorithm gets the updated position information after each iteration, and finally the error generated by the system is substituted into the fitness function, and then its fitness value is calculated. The obtained fitness value is passed to BAS and compared with the set threshold to obtain the optimal parameters of the PIR, and then the decomposition of the three dimensions of the position is assigned to k_p k_i and k_r to obtain the optimal parameters k_p k_i and k_r. The microprocessor implements the PIR control according to the determined optimal QPIR control parameters (k_p k_i k_r) modulates the PWM signal and outputs it to the driver circuit. The driver circuit module receives the PWM control signal from the microprocessor and outputs the compensation current accordingly to implement harmonic compensation for the distribution network.

4 UPQC simulation results and analysis

(1)Main parameters of the UPQC system

In order to verify the feasibility of the UPQC harmonic control strategy of the quasi-PIR controller based on the Beetle Antennae Search Algorithm selected for this design. The simulation model of harmonic compensation detection of UPQC was built use MATLAB /Simulink simulation software, and its simulation parameters were set as shown in Table 1.

To further verify that the BAS optimization algorithm has high convergence accuracy and fast convergence speed, the basic NNA optimization algorithm is used to optimize the control parameters and compare the adaptation curves obtained from its optimization with those obtained from BAS optimization, and the comparison results are shown in Fig. 8 .

Table 1
Main parameters of the UPQC system

Major parameters	Value/Unit
Grid voltage	220V
DC-side capacitance voltage	800V
DC-side capacitance	260μF
Series side filter inductor	2.5mH
Series side filter capacitor	50μF
Shunt side filter inductor	3mH
Series transformer ratio	1:1
Switching frequency	10kHz

(2)Simulation and Analysis

As can be seen from the Fig. 8, the BAS optimization algorithm and the basic NNA optimization algorithm have similar accuracy and both can converge to a stable fitness value. However, the basic NNA optimization algorithm is easy to fall into the local optimum in the iterative process, and the convergence process is highly variable and less stable. In contrast, the BAS optimization algorithm prevents the particles from falling into local optimum during the iteration process by reducing the search interval. Therefore, using BAS algorithm for

dominant control parameter optimization can ensure the accuracy and stability of the parameter optimization solution.

In order to ensure the accuracy of the analysis results, the stability simulation of the current loop control parameters was carried out, and the root mean square value of the current obtained by the NNA-PI control method and the root mean square value of the current obtained by the BAS-QPIR control method were compared and verified in UPQC, and the results are shown in Fig. 9.

The results are shown in the Fig. 9. The waveforms of the output currents of the devices show different degrees of fluctuations, and the RMS values of the output currents clearly show the periodic oscillations in the output currents of the grid-controlled devices using the NNA-PI control method. Its dynamic performance has been significantly reduced, and the system cannot maintain stable operation after a disturbance. A more destabilizing phenomenon is presented. And it can be observed by the root-mean-square value of output current that the system with BAS-QPIR control method has less perturbation in current change, and its output current changes weakly, showing a significantly better dynamic performance than the NNA-PI control method.

In the UPQC system, the step response of the PI controller based on the neural net-work algorithm is obtained, and the step response curve of the PI controller opti-mized by the neural network algorithm is shown in Fig. 10a. The step response of the system reflects the dynamic characteristics of the system to a large extent, and it can be seen from the figure that the step response curve has an overshoot amount, which will make the regulation time of the system too long, and if the overshoot amount is too large, it also damage the system and will affect the compensation effect of the UPQC system for harmonic currents.

In the UPQC system, the step response of the QPIR controller based on the aspen whisker algorithm, the response curve is obtained as shown in Fig. 10b. From the step response curve of the QPIR controller optimized by the aspen whisker algorithm, it can be seen that its step response does not contain overshoot, and the former PI con-troller step response reaches the system set value in basically the same time, but there is overshoot in the former optimization method, which will make the system unstable. In a comprehensive comparison, the latter is superior to the former control method and has better control performance, which can make the UPQC system perform fast compensation and improve the com-pensation effect.

In the UPQC simulation environment, the current waveform at the load of the PV microgrid is measured as shown in Fig. 11a.As can be seen from the figure, the current waveform shows obvious sawtooth waveform, which indicates that the harmonic current pollution in the distribution network is serious, and the main cause of current pollution is the 5th, 7th, 9th and other odd harmonics, in addition to the three-phase rectifier bridge load is a non-linear load is very easy to cause harmonics.

Figure 11b depicts the PI controller compensated microgrid current waveform in the PV environment after 0.1 seconds of UPQC compensation. The waveform has become more sinusoidal and smoother, but there are still some burrs present, particularly at the peaks and valleys. These burrs indicate that while the PI control method in the UPQC system can compensate for harmonics, the compensation effect is not ideal.

At 0.13 seconds the UPQC system starts to intervene to compensate, and the obtained microgrid current waveform after compensation by QPIR controller in PV environment is shown in Fig. 11c.

After compensation, the waveform is significantly improved, and the waveform at the load tends to be sinusoidal, and the response time and speed meet the requirements of compensation. Compared with the waveform after compensation by PI controller based on neural network algorithm, the burr is less and the waveform is smoother, which indicates that the harmonic current can be accurately compensated by using quasi- PIR control method in UPQC system, and the compensation strategy and control method can make the harmonics well suppressed.

The current waveform at the load in the wind energy environment is measured in the UPQC simulation environment. Figure 12a displays the waveform, which appears irregular and trapezoidal. This suggests significant harmonic current pollution in the distribution network. To maintain stable grid operation in real time, UPQC compensation is necessary.

From the moment of 0.02 seconds, after compensation by the UPQC system, the PI control compensation waveform of the microgrid current in the wind energy environment is shown in Fig. 12b. The effect of PI control in UPQC is not ideal.

Starting from 0.02 seconds, the harmonic currents are compensated in the UPQC system based on the QPIR control method, and the waveforms of the microgrid currents after compensation by the QPIR controller in the wind energy environment are obtained as shown in Fig. 12c.

It can be seen that the compensated waveforms are significantly improved and close to smooth sine waves, and the waveform surfaces are smoother and less burrs compared with the waveform plots at the load after compensation by the PI controller in the wind energy environment, indicating that the harmonics can be well suppressed by the UPQC system after compensation.

Another important index to measure the operational performance of UPQC is the harmonic control effect of the whole system after treatment. Therefore, in order to further verify the effect of the control parameter optimization results obtained in this paper on the harmonic treatment of microgrid, the system harmonic treatment effect under different operating conditions is analyzed. The harmonic current distortion rate of each node of the system was compared and analyzed. The current distortion of each node is shown in Fig. 13.

According to the results of current distortion rate comparison at each node of the system, it can be seen that the voltage distortion of the nodes in the distribution network other than the nodes near the power supply exceeds the standard severely due to the influence of decentralized harmonic sources, which makes the system unable to work normally and is not conducive to the normal operation of the system. In contrast, the node voltage distortion rate of the system is significantly reduced after adopting BAS-QPIR control method, which is good to weaken the influence of its harmonic rule and enable the system to operate stably and ensure that the harmonic content in the treatment area meets the requirements, which makes the system power quality significantly improved.

It should be added that the filtering of harmonics using the NNA-PI control method in Fig. 14 requires a compromise between the filtering effect and the dynamic response, and although the end frequency is set to 15 Hz to filter the AC component, it does not suppress the harmonics ideally. Figure 14 shows the analytical spectrum of the harmonic content in the fundamental wave detected by the two schemes. It is clear that based on the filtering effect of the NNA-PI control method, the 3rd harmonic is still 0.79%; while the 3rd harmonic is only 0.16% after filtering with the BAS-QPIR control method. Therefore, compared with the filtering effect of the NNA-PI control method, the filtering effect based on the BAS-QPIR control method in this paper not only controls the dynamic response time to within half an operating frequency cycle, but also has a better filtering effect.

As shown in Fig. 15a .The current spectrum of AC microgrid before compensation, the harmonic distortion rate THD value before compensation is as high as 32.61%, which indicates serious harmonic current pollution, and also makes the grid voltage waveform distortion, when a large number of loads and

equipment with high harmonic content operate, it will lead to positive and negative half-cycle asymmetry of the power supply circuit, which will endanger the safe operation of the power system, and then UPQC is needed to compensation.

After compensation by the UPQC system, the frequency spectrum after compensation based on the PI control of neural network algorithm is obtained as shown in Fig. 15b.

The compensation reduces the THD to 4.84% and harmonics are significantly improved, which meets the requirement of compensation within 5%. It shows that the compensation by the UPQC system can make the microgrid environment with certain anti-interference performance and dynamic performance, and improve the stability and anti-interference of the system to a certain extent.

The compensation reduces the THD to 4.84% and harmonics are significantly improved, which meets the requirement of compensation within 5%. It shows that the compensation by the UPQC system can make the microgrid environment with certain anti-interference performance and dynamic performance, and improve the stability and anti-interference of the system to a certain extent.

After the compensation by UPQC intervention, the current spectrum plot after compensation by the QPIR controller based on the BAS algorithm is obtained as shown in Fig. 15c, which makes the THD drop to 2.68% and the harmonics are significantly improved, compared with the current spectrum of the grid after compensation by the PI controller method based on the neural network algorithm, the latter makes the THD drop to 2.68%, which has a better compensation effect and greatly reduces the harmonic distortion rate THD value, which indicates that the harmonic control strategy of the quasi-PIR controller based on the aspen whisker algorithm in UPQC can make the microgrid have better anti-interference performance and dynamic performance.

5 Conclusion

Since the presence of a large number of nonlinear electronic components inside the microgrid can lead to a large number of harmonics in the microgrid, which can have a serious impact on the power quality of the microgrid, this paper proposes a harmonic control method using UPQC in the mi-crogrid with a QPIR controller optimized by the BAS algorithm. The BAS algorithm adjusts and optimizes the required parameters of the QPIR controller. Comparison with the adaptation curves obtained by the NNA optimization algorithm shows that the BAS optimization algorithm can ensure the accuracy and stability of the parameter optimization solution by reducing the search interval of the particles and preventing them from falling into local optimum during the iteration process. Simulations are performed in MATLAB/Simulink and compared with simulation experiments using the NNA-PI control method in the operating environments of wind energy and photovoltaic, respectively, and the results show that the UPQC harmonic control strategy using the BAS-QPIR control method is imitated for practical engineering applications and provides a new method for solving the UPQC harmonic problem. The strategy can detect various sub-frequency harmonic currents and selectively compensate for specific sub-frequency harmonics. In addition, it improves the dynamic response performance of the system and effectively improves the power quality of the microgrid.

Declarations

Funding Statement:

Supported by Open Project of Jiangsu Key Laboratory of Power Transmission & Distribution Equipment Technology (2021JSSPD12)

Supported by Talent projects of Jiangsu University of Technology (KYY20018)

Supported by Graduate practice innovation program of Jiangsu University of Technology (XSJCX21_32)

Conflicts of Interest:

The authors declare that they have no conflicts of interest to report regarding the present study.

References

1. Xu F, Zheng Q , Ni X , et al. Fault location method of distribution network under distributed power supply access[C]// 2019 *IEEE Sustainable Power and Energy Conference (iSPEC).* IEEE, 2020.
2. Vimalrose S, Kumar M. Variable DC part Voltage of DSTATCOM for enhancing power quality of microgrid[C]// 2019 International Conference on *Power Electronics Applications and Technology in Present Energy Scenario (PETPES).* 2019.
3. GUO, BIN, SU, MEI, SUN, YAO, et al. Cost-Effective DC Current Suppression for Single-Phase Grid-Connected PV Inverter[J]. *IEEE journal of emerging and selected topics in power electronics,*2021,9(2):1808-1823. DOI:10.1109/JESTPE.2020.3029393.
4. He J, Liu X, Lei M , et al. A Broad Frequency Range Harmonic Reduction for Cascaded-Power-Cell-Based Islanded Microgrid with Lumped PCC Filter[J]. *IEEE Transactions on Power Electronics,* 2020, 35(9):9251-9266.
5. Sukhesh H R, Senthil V U. Cascade PI-Fuzzy Based Position Optimization of Nonal Switched UPQC with DG for Power Quality Enhancement in IEEE 14 Bus System[J]. *WSEAS Transactions on Circuits and Systems,* 2021(20-).
6. Abdalaal R, Ho C. System Modeling and Stability Analysis of Single-Phase Transformerless UPQC Integrated Input Grid Voltage Regulation[J]. I*EEE Journal of Emerging and Selected Topics in Industrial Electronics,* 2021, PP(99):1-1.
7. Zhao X, Zhang C, Guo X, et al. Novel power flow analysis method based on impedance matching for UPQC with grid voltage fluctuations and unbalanced loads[J]. *IET Power Electronics,* 2020, 13(2).
8. Chen Q. A Control Strategy of Islanded Microgrid with Nonlinear Load for Harmonic Suppression[J]. *IEEE Access,* 2021, PP(99):1-1.
9. He L, Li Y, Guerrero J M, et al. A Comprehensive Inertial Control Strategy for Hybrid AC/DC Microgrid With Distributed Generations[J]. *IEEE Transactions on Smart Grid,* 2019, PP.(99):1-1.

10. YURKEVICH, V. D.PIR-Controller Design Based on Time-Scale Separation Method and Internal Model Principle for Harmonics Disturbanes Suppression[J]. *Optoelectronics, Instrumentation and Data Processing,*2021,57(4):363-370. DOI:10.3103/S8756699021040130.
11. Kh A, Mmo A, Stm B, et al. Online harmonic extraction and synchronization algorithm based control for unified power quality conditioner for microgrid systems[J]. 2022.
12. Wang Liang, Lu Yemin. Comparative study on the control of constant pressure water supply PID system by fuzzy and tianniuxu optimization algorithms [J]. *Industrial control computer,* 2022, 35 (03): 77-79.
13. Zhang W, Cao B, Nan N, et al. An adaptive PID-type sliding mode learning compensation of torque ripple in PMSM position servo systems towards energy efficiency[J]. *ISA Transactions,* 2020.
14. Charvat G L, Mindell D A. Polarization techniques for suppression of harmonic coupling and associated systems, dev-ices, and methods, US11050133B2[P]. 2021.
15. Siddique A B, Munsi M S, Sarker S K, et al. Voltage and Current Control Augmentation of Islanded Microgrid using Multifunction Model Reference Modified Adaptive PID Controller[J]. *International Journal of Electrical Power & Energy Systems,* 2019, 113(DEC.):492-501
16. Reddy P M, Reddy A S, Sarvesh B. Hybrid ANFIS-FA-based control strategy for UPQC - power quality enhancement in smart grid[J]. *International Journal of Power Electronics,* 2021, 13(4):399.
17. Lei T , Riaz S , Zanib N , et al. Performance Analysis of Grid-Connected Distributed Generation System Integrating a Hybrid Wind-PV Farm Using UPQC[J]. *Complexity,* 2022, 2022.
18. Zhu X, Wang H , Yue X , et al. Low Frequency Ripple Removal Method for LLC Converter Based on Quasi-PIR Controller[C]// IECON 2019 - 45th Annual Conference of the IEEE Industrial Electronics Society. *IEEE,* 2019.
19. Yu J, Xu Y, Li Y, et al. An Inductive Hybrid UPQC for Power Quality Management in Premium-Power-Supply-Required Applications[J]. *IEEE Access,* 2020, P P.(99):1-1.
20. Bueno-Contreras H, Ramos G A, R Costa-Castelló. Power Quality Improvement through a UPQC and a Resonant Observer-Based MIMO Control Strategy[J]. *Energies,* 2021, 14.
21. Li S, Han W, Li X , et al. Harmonic Suppression Strategy of Photovoltaic Grid Connected Inverter Based on Repetitive and PI Control[J]. *Journal of Physics: Conference Series,* 2021, 2136(1):012032-1.
22. Lee W G, Nguyen T T, Kim H M. Multiagent-Based Distributed Coordination of Inverter-Based Resources for Optimal Operation of Microgrids Considering Communication Failures[J]. E*nergies,* 2022, 15.
23. Chen J,Zeng Q, Li, et al. A Coordination Control Method for Multi-terminal AC/DC Hybrid System Based on MMC Transmission Technology[C]// 2019 IEEE 10th International Symposium on *Power Electronics for Distributed Generation Systems (PEDG).* IEEE, 2019.
24. Wang Y , Lin X , Liu Y , et al. Research on AGV Path Planning Method Based on Improved BAS Algorithm[J]. *Electric Engineering,* 2019.

Figures

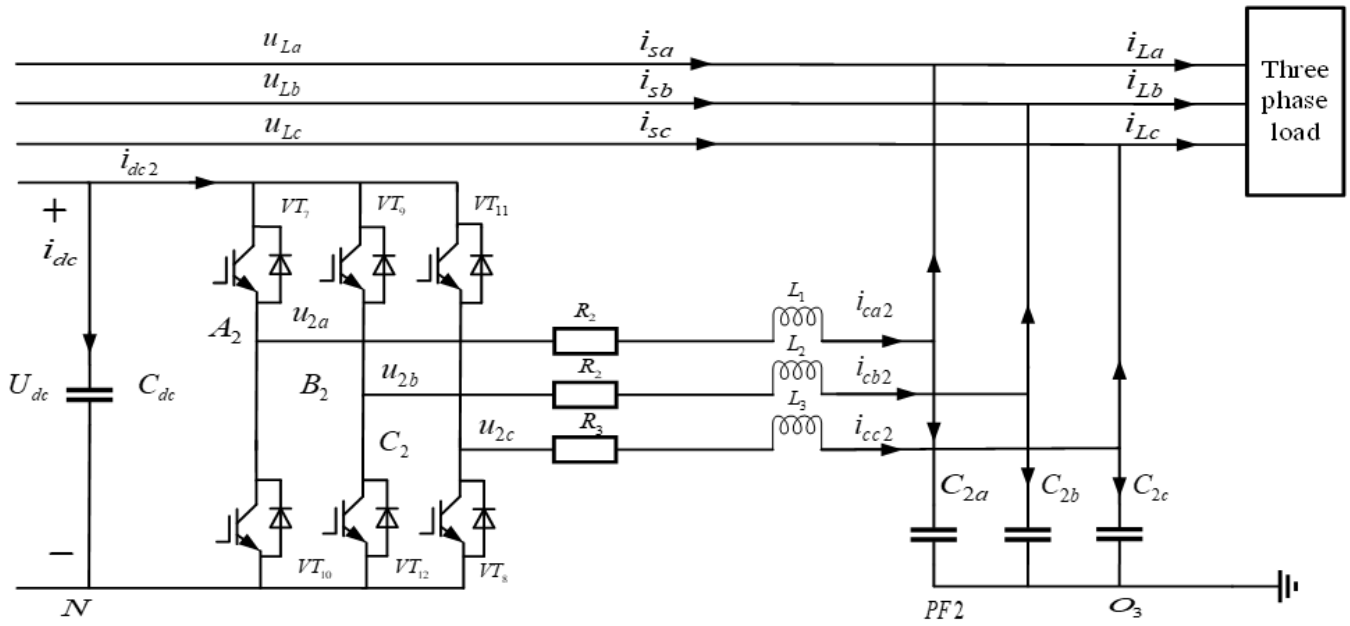

Figure 1

Parallel unit topology circuit diagram

Fig. 2

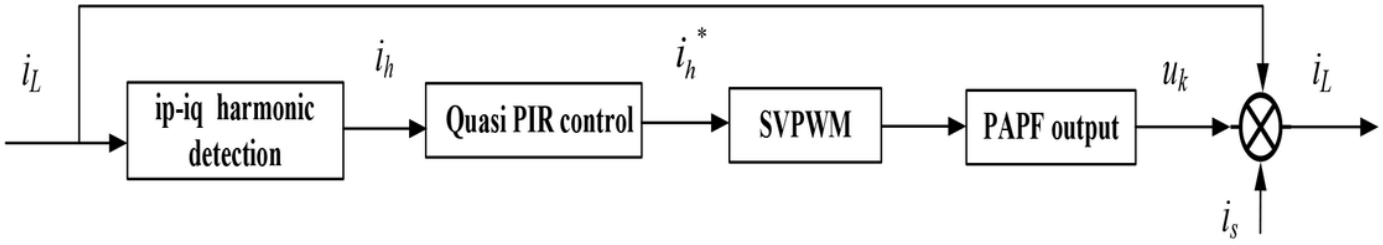

Figure 2

Principle diagram of UPQC harmonic current detection and compensation

Fig. 3

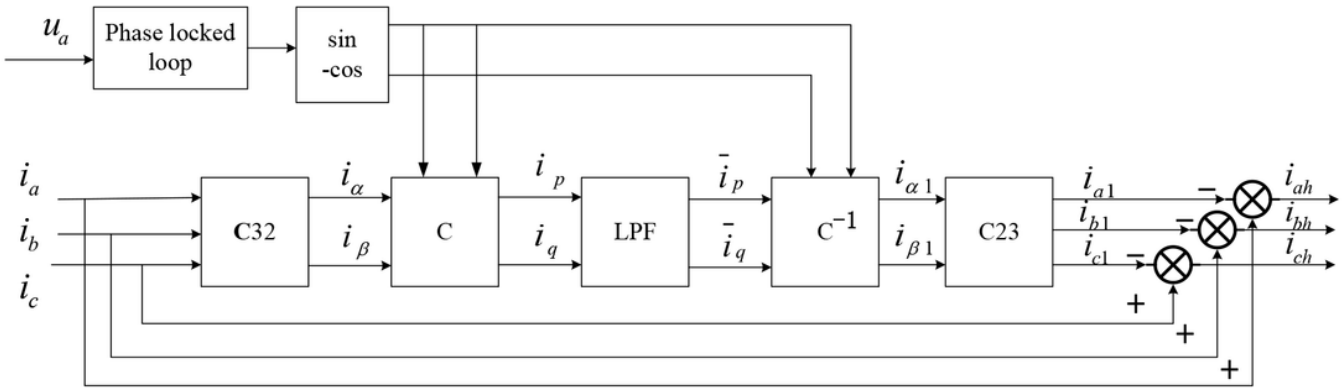

Figure 3

Principle diagram of UPQC harmonic detection based on ip-iq

Fig. 4

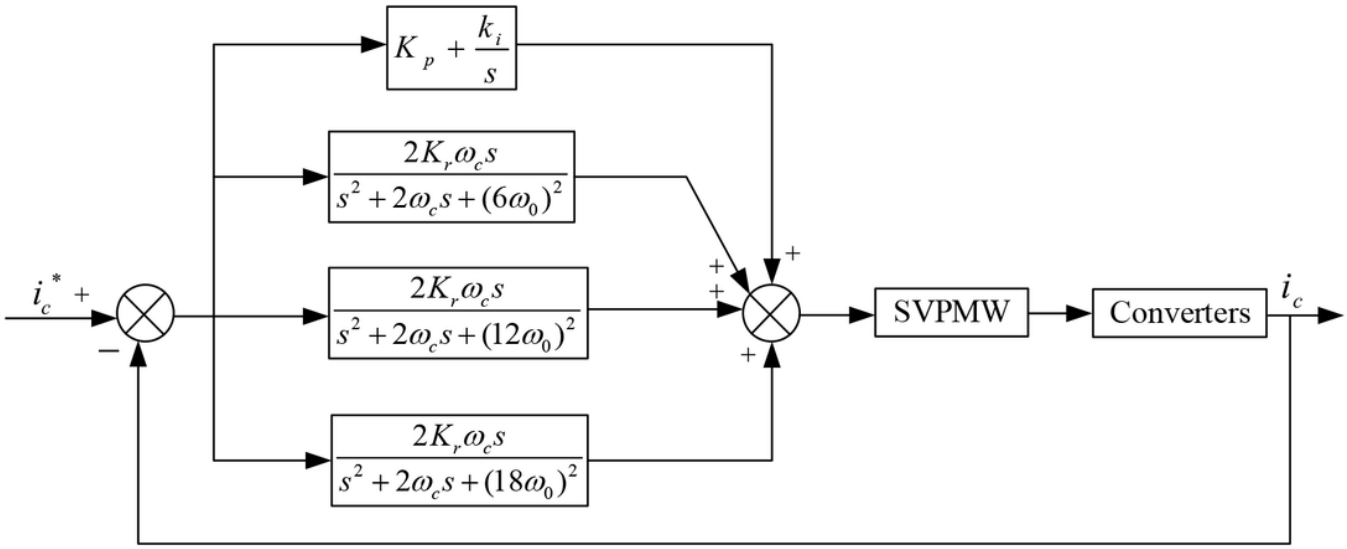

Figure 4

Block diagram of the quasi-PIR control principle

Fig. 5

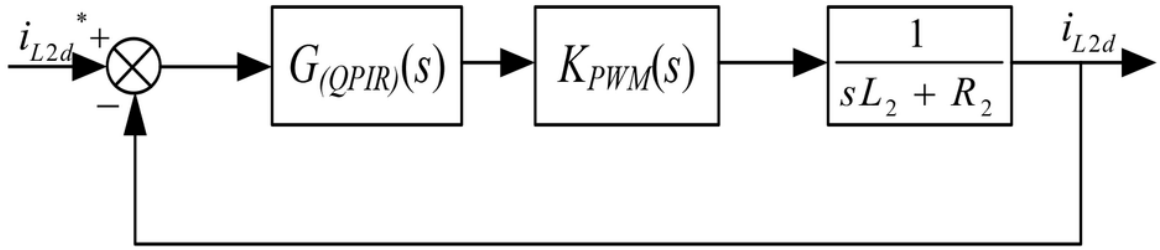

Figure 5

Simplified control block diagram of d-axis current loop

Fig. 6

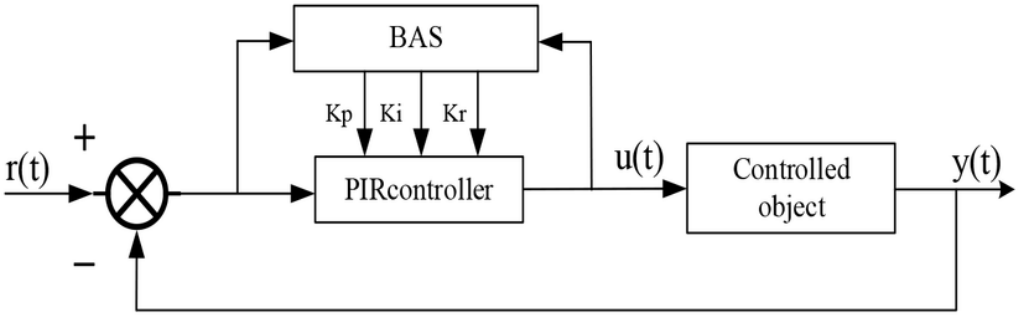

Figure 6

Block diagram of the quasi-PIR parameter adjustment system for BAS

Fig. 7

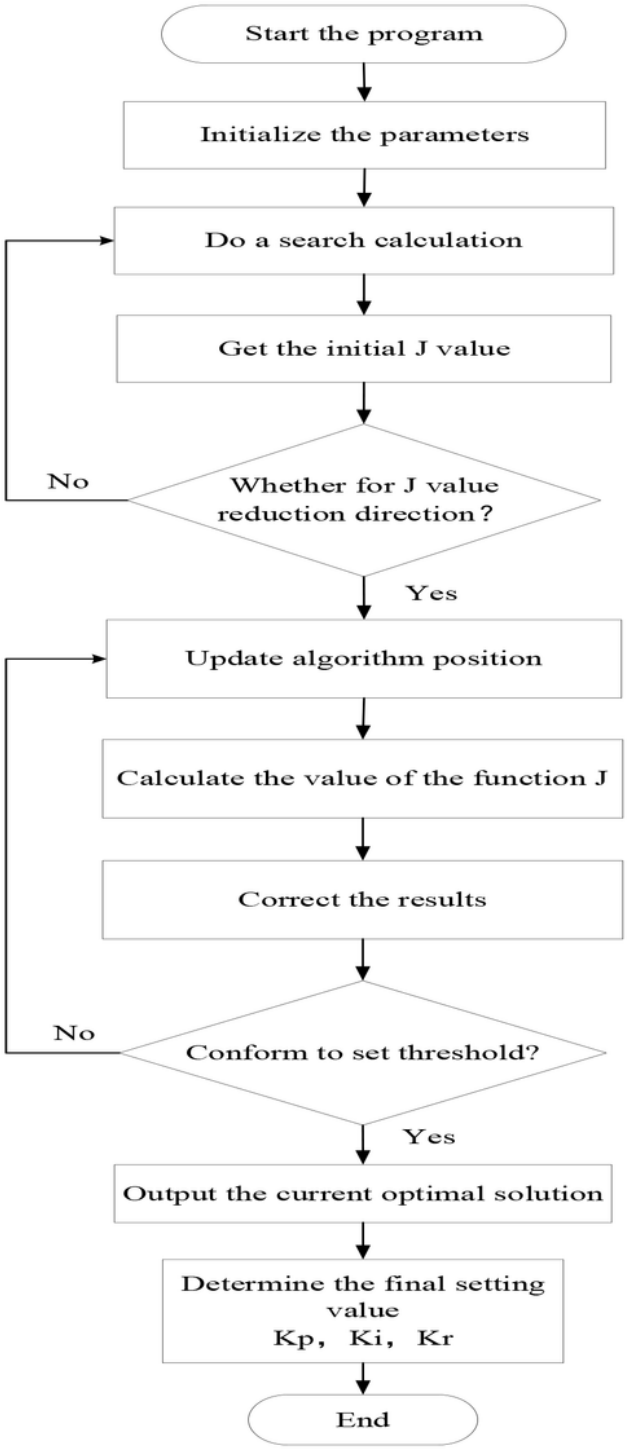

Figure 7

BAS algorithm rectification flow chart

Fig. 8

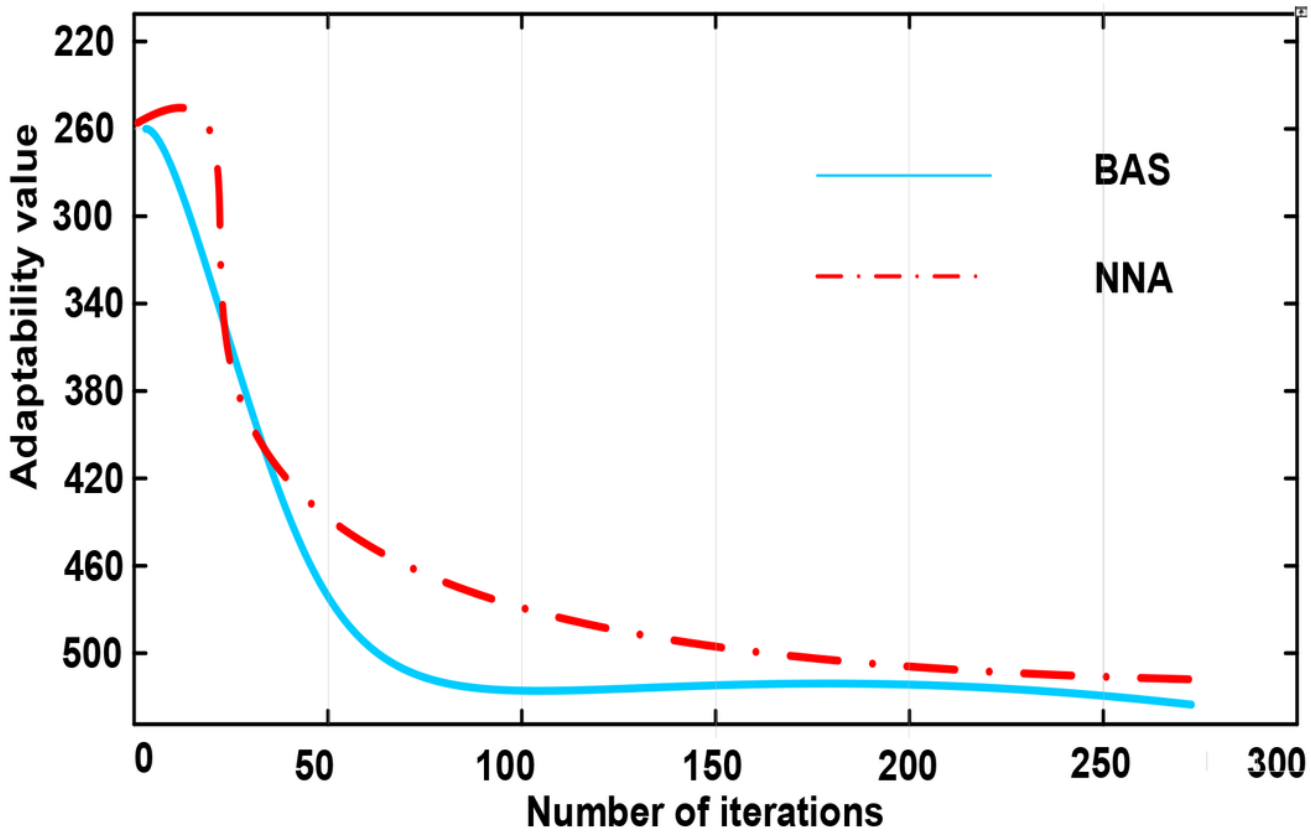

Figure 8

Adaptation curves of BAS and NNA

Fig. 9

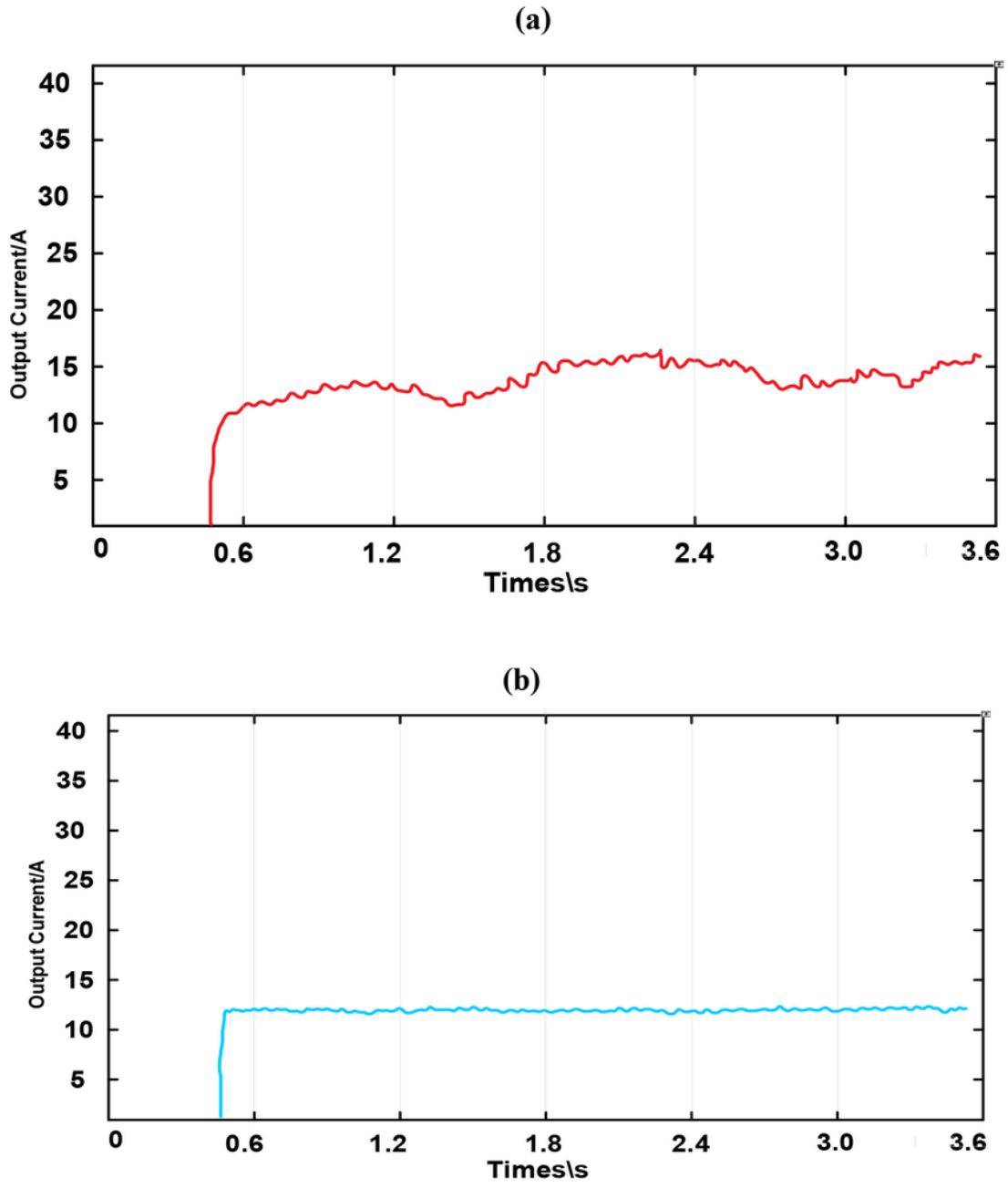

Figure 9

Output current root mean square value; **a** NNA-PI output current root mean square value and **b** BAS-QPIR output current root mean square value

Fig.10

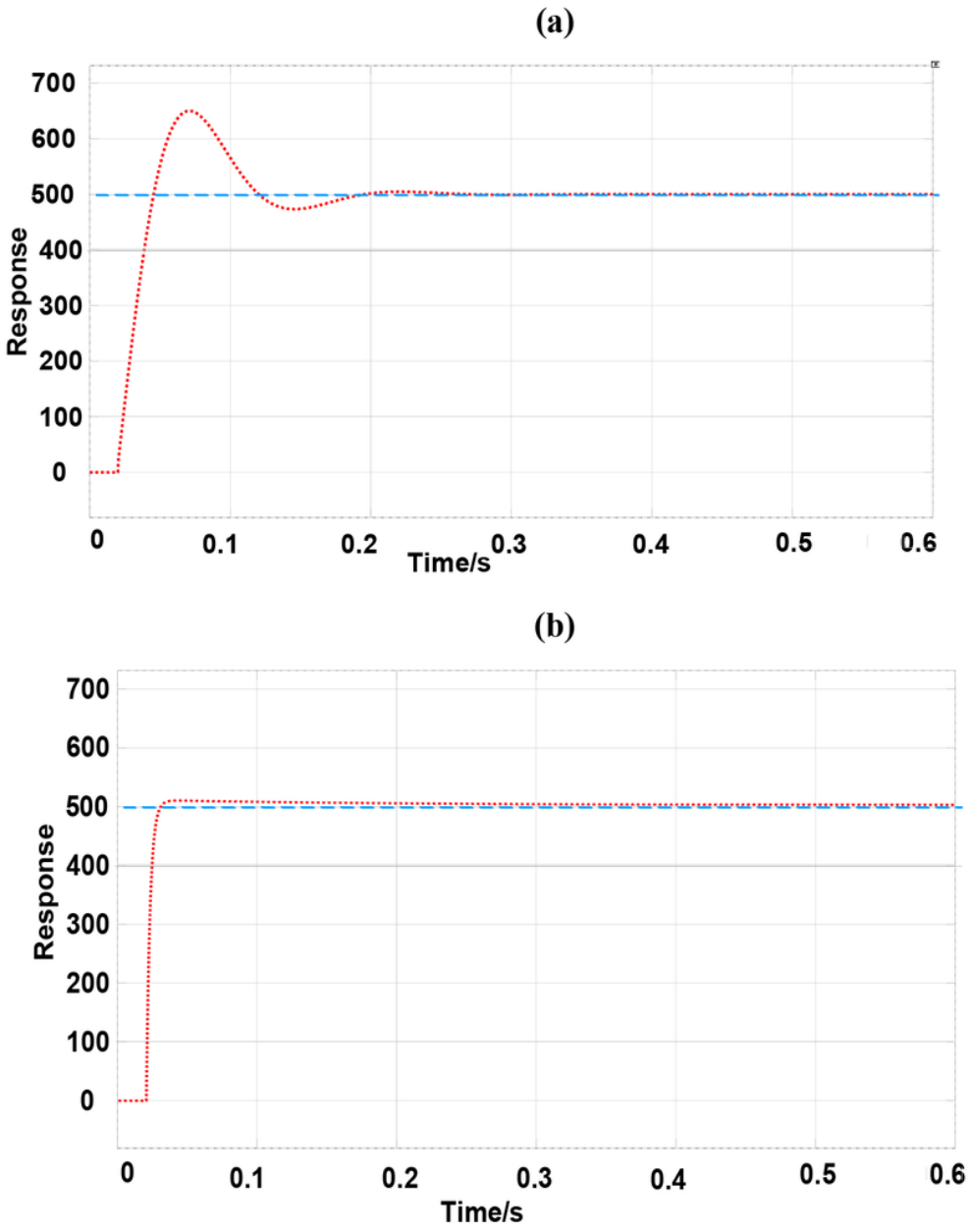

Figure 10

Step response curve

a NNA-PI Step response curve and **b** BAS-QPIR control Step response curve

Fig. 11

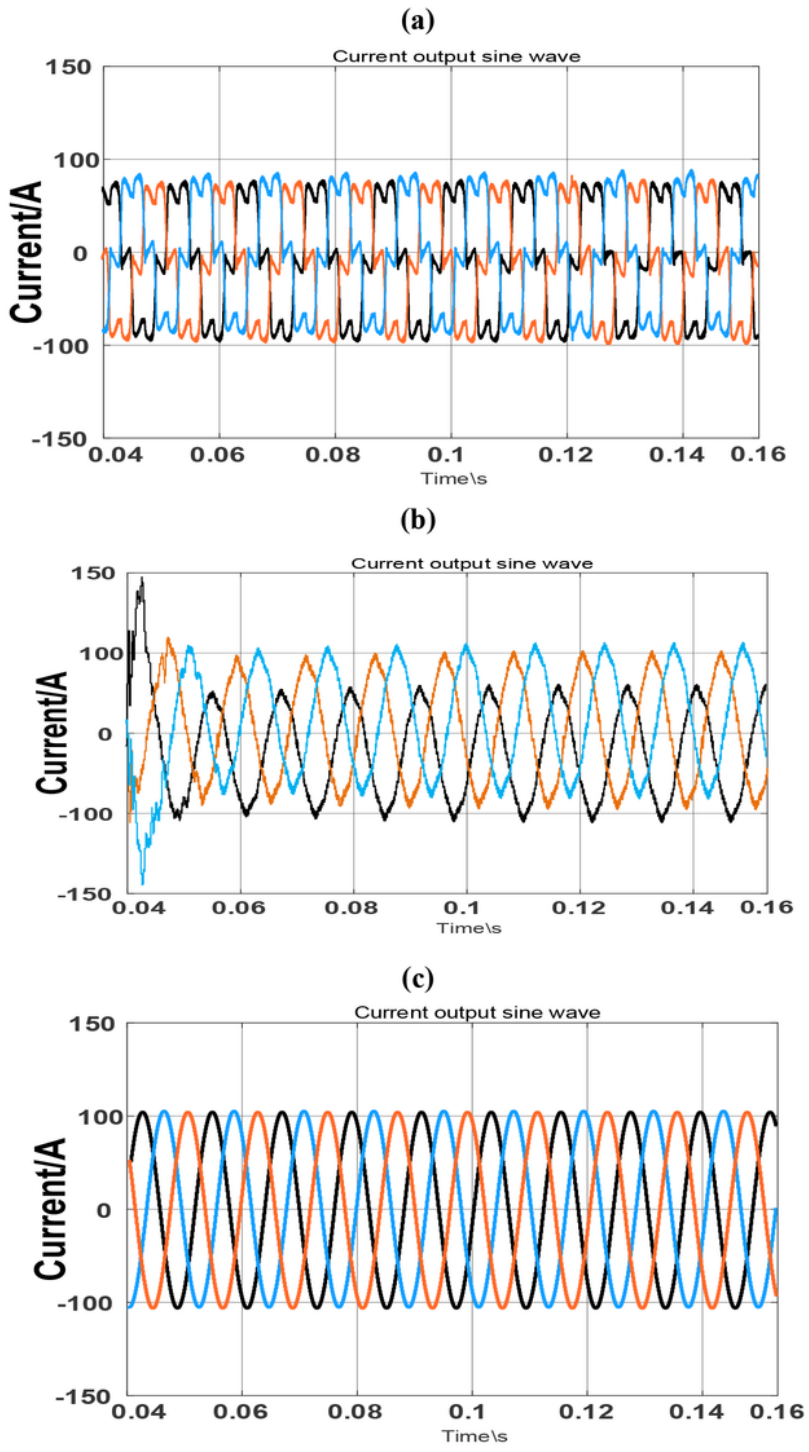

Figure 11

Microgrid Current Waveforms

Before and After Compensation in PV: **a** Current waveform of microgrid before compensation, **b** PI algorithm control in PV and **c** Beetle antennae search algorithm in PV

Fig. 12

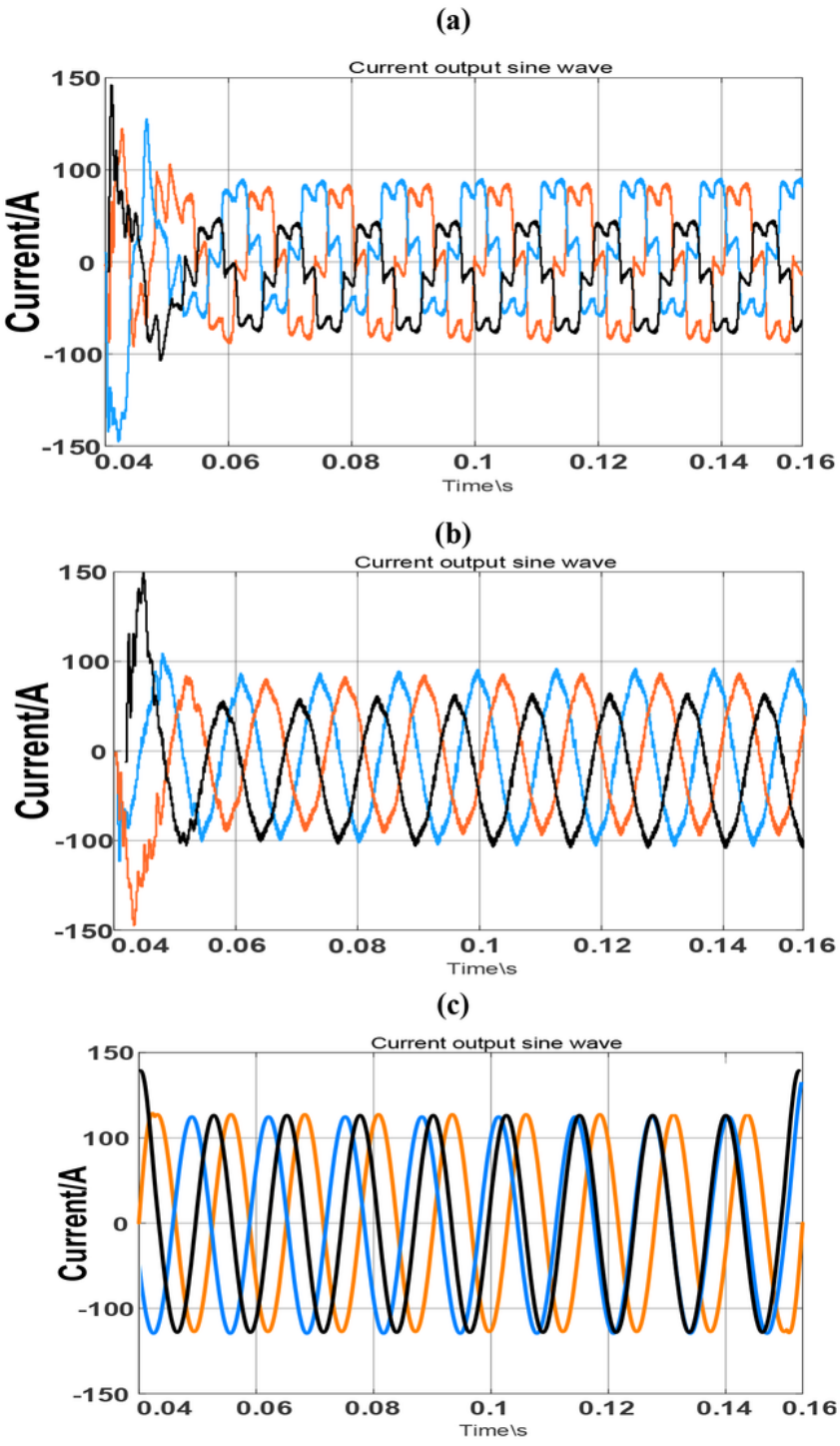

Figure 12

Microgrid Current Waveforms Before and After Compensation in wind: **a** Current waveform of microgrid before compen-sation; **b** PI algorithm control in wind and **c** Beetle antennae search algorithm in wind

Fig. 13

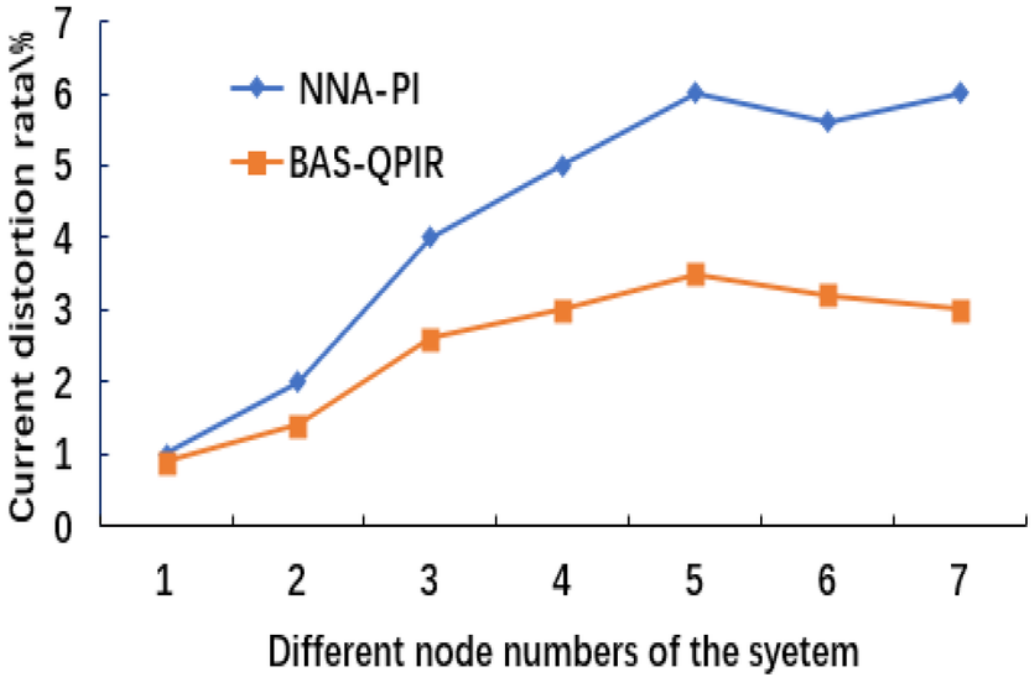

Figure 13

Harmonic current distortion rate at each node of the system

Fig.14

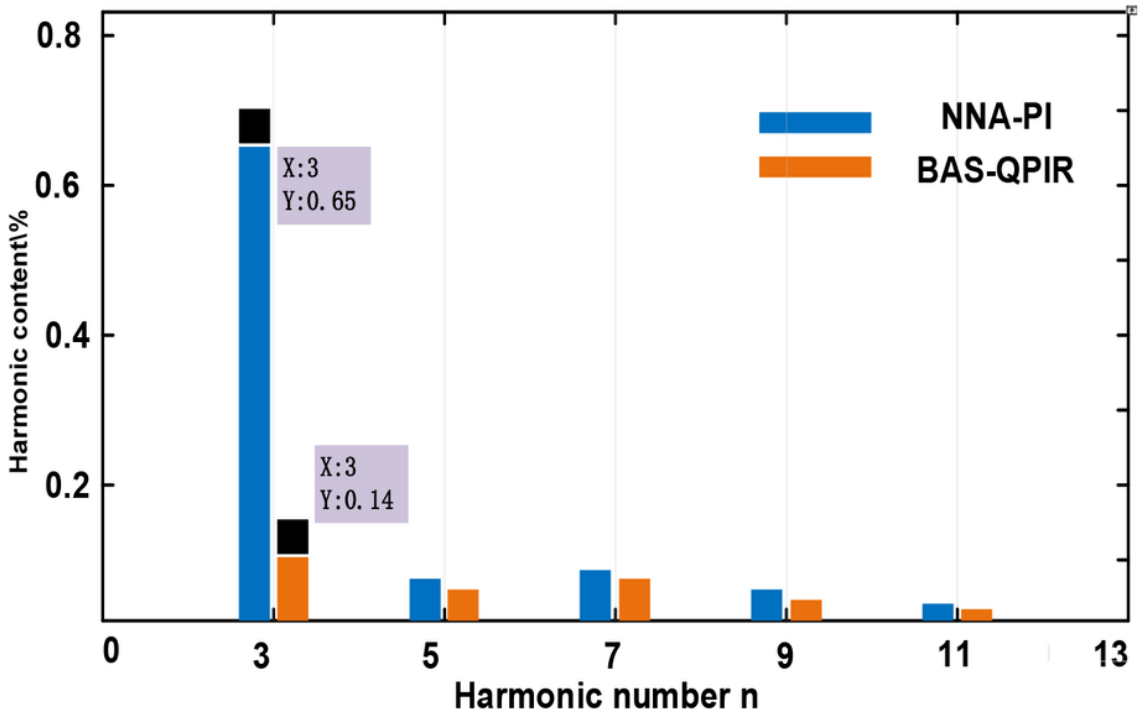

Figure 14

Harmonic content in fundamental wave

Fig. 15

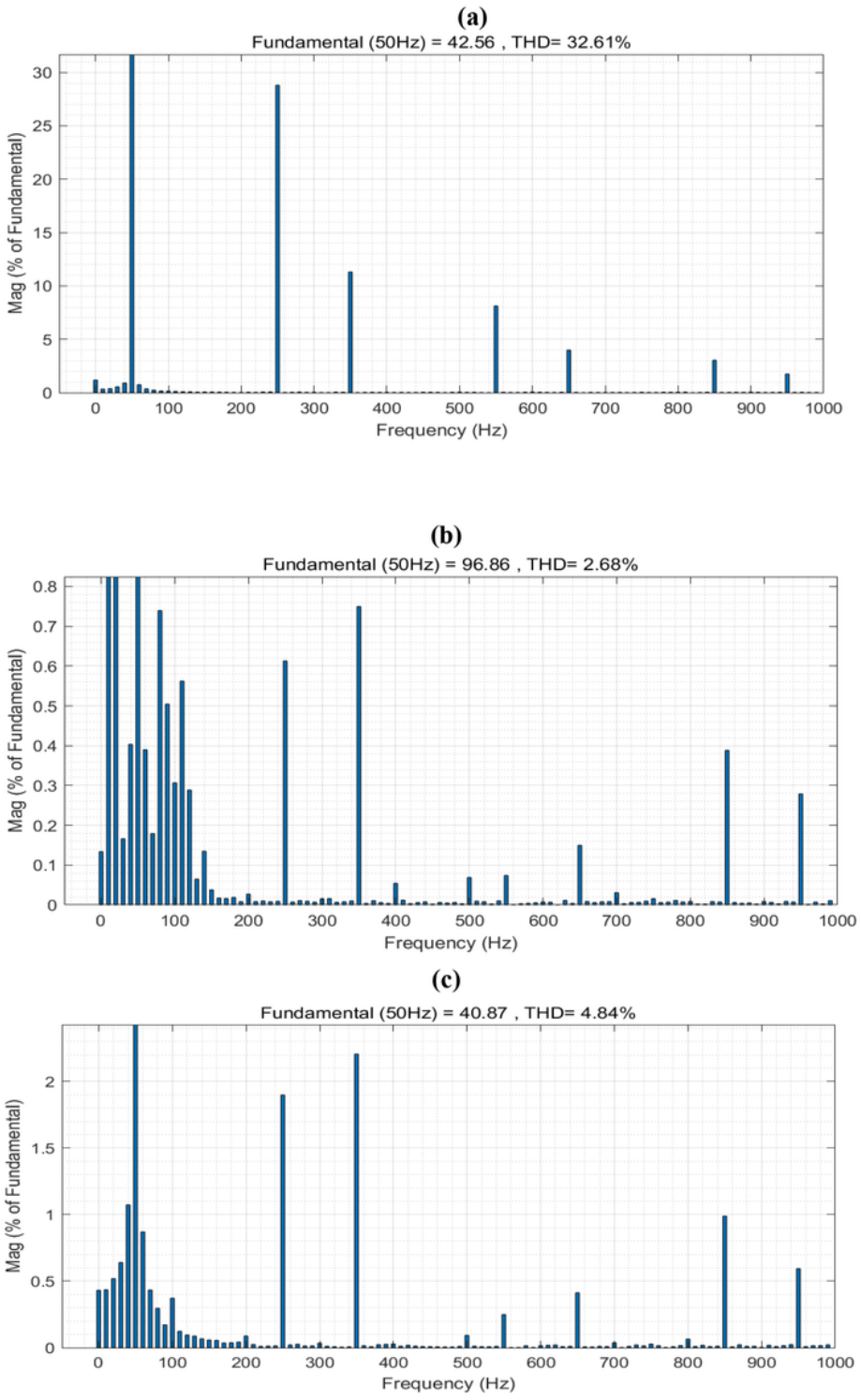

Figure 15

Load voltage spectra:

a Voltage spectrum before governance

b Traditional PI NNA-PI control method and **c** BAS-QPIR control method